Supplementary Material (ESI) for Lab on a Chip

Three-dimensional (3D) continuous particle focusing in a microfluidic channel via standing surface acoustic waves (SSAW)

Jinjie Shi,[a,b] Shahrzad Yazdi,[a,c] Sz-Chin Steven Lin,[a] Xiaoyun Ding,[a] I-Kao Chiang,[a] Kendra Sharp,[d] and Tony Jun Huang[*a,c]

[a] *Department of Engineering Science and Mechanics, The Pennsylvania State University, University Park, PA 16802, USA. Fax: 814-865-9974; Tel: 814-863-4209; E-mail: junhuang@psu.edu*
[b] *The DOW Chemical Company, Spring House Technology Center, Spring House, PA, 19477, USA.*
[c] *Department of Mechanical and Nuclear Engineering, The Pennsylvania State University, University Park, PA 16802, USA.*
[d] *Department of Mechanical, Industrial, and Manufacturing Engineering, Oregon State University, Corvallis, OR, 97331, USA*

1. Device Fabrication

The fabrication process and the final device are shown in Figure S1. A thin layer of photoresist (PR) SPR3012 was spin-coated on a Y+128° X-propagation lithium niobate ($LiNbO_3$) wafer, patterned by UV light source, and developed in a photoresist developer (MF CD-26, Microposit). After depositing a PR layer, lithography was used to form two parallel IDTs, followed by metal deposition (50Å/800Å, Cr/Au) and a lift-off process. The two parallel gold IDTs have a period of 100 μm and an electrode width of 25 μm. A PDMS microchannel (1.3 cm, 50 μm x 50 μm) was then fabricated by standard soft-lithography and mold-replica techniques [S1]. The silicon mold used in our experiments was patterned by photoresist Shipley 1827 (MicroChem, Newton, MA) and etched by a Deep Reactive Ion Etching (DRIE, Adixen, Hingham, MA) process. The silicon mold was coated with 1H,1H,2H,2H-perfluorooctyl-trichlorosilane (Sigma Aldrich, St. Louis, MO) in a vacuum chamber during the demolding process to moderate surface energy and damage to the PDMS microchannel. Sylgard™ 184 Silicone Elastomer Base and Sylgard™ 184 Silicone Elastomer Curing Agent (Dow Corning, Midland, MI) were combined (11:1 weight ratio), cast onto the silicon mold, and cured at 70 °C in an oven for 30 min (curing times varied for different levels of hardness). The inlets and outlets of the microchannel were created using a silicon carbide drill bit. The bonding regions were stimulated with oxygen plasma (oxygen flow rate: 50 sccm; chamber pressure: 750 mTorr; and power: 150 W) to improve the bonding between

the PDMS channel and the SAW substrate. A drop of ethanol was placed between the piezo-substrate and the microchannel to facilitate the alignment between the channel and SAW substrate. Once the channel was aligned, the ethanol was removed in a vacuum chamber at 50°C for 15 min. Finally, polyethylene tubing (Becton Dickson, Franklin Lakes, NJ) was inserted into the inlet and outlet of the PDMS microchannel. To generate continuous flow, the tubing was also connected to a syringe pump (KDS 210, KD scientific, Holliston, MA).

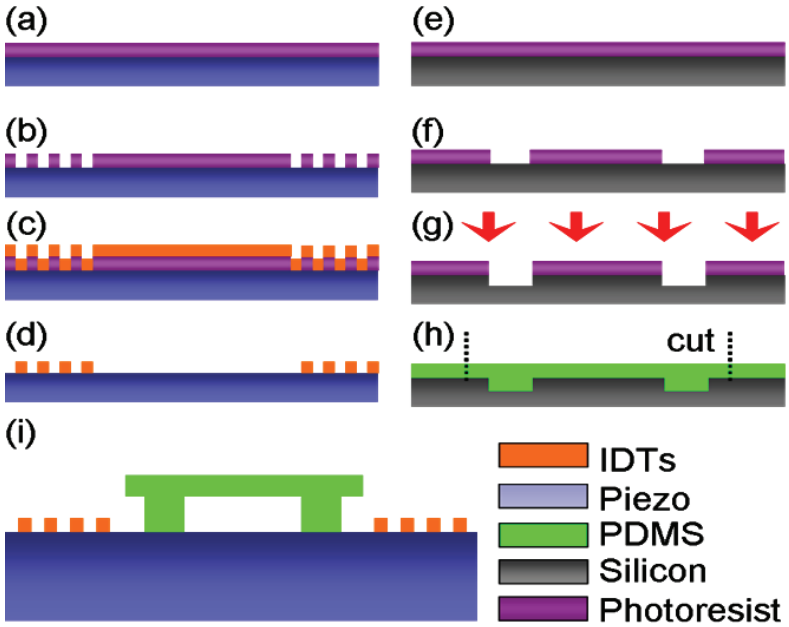

Fig. S1 Device fabrication process. (a–d) Fabrication of the SAW substrate including a metal deposition process and a following lift-off process. (e–h) A soft-lithography process was used to fabricate PDMS-based microchannels. (i) The alignment and bonding between the SAW substrate and the channel.

2. Supplemental Video

"Top-view video of 3D focusing of fluorescent microparticles." The movie is in real time.

3. Effect of channel height on the focusing point

The width (w) and height (h) of the channel are important parameters in designing our SSAW-based device. The width of the channel determines how many pressure nodes lie in the channel. Particles with $\varphi > 0$ (where φ is defined in equation 4 of the manuscript) move to the pressure nodes. For particle focusing, therefore, we only need one pressure node. Since

for flow cytometry and other applications of particle focusing, it is more desirable to have the particles focused in the middle of the channel. Hence, the microchannel should be placed precisely in between the IDTs with the same distance from each IDT. The width of the channel should be half of the wavelength or less. This guarantees existence of a pressure node in the middle of the channel.

The vertical position of the focused particles is dictated by the distribution of acoustic energy in the pressure-nodal plane. Regardless of the channel height, the maximum acoustic energy region within the pressure-nodal plane is confined to the height of a triangular-shaped area depicted in Fig. 5(b). The size of this triangular-shaped area is dictated by the Rayleigh angle as well as the width of the channel, but not the channel height. Therefore, since Rayleigh angle and channel width are fixed parameters, the height of the triangular-shaped area is constant.

We have conducted some computational studies to address the effect of channel height on the focusing region. In addition to the 100 μm height used in our experiments, heights of 50, 80, 125, and 155 μm were added for these additional studies. Figure S2 shows the simulation results conducted for various channel heights. For each height, time-averaged velocity square in the *x*-direction (V_x^2), *y*-direction (V_y^2), and time-averaged velocity squared in the *x*-direction (V_x^2) and *y*-direction (V_y^2) within the middle plane (x=25 μm) is plotted. The focal point in the vertical direction depends on the location of maximum kinetic energy point within the pressure nodal plane, namely the aforementioned triangular region. Since V_x^2 is zero in the pressure nodal plane, the maximum kinetic energy is found at the maximum of V_y^2. This maximum can be calculated from the line plots in each subsection in Fig. S2. Figure S2(e) shows the normalized position of focal point (to channel height) as a function of the channel height. Overall, the normalized focal position decreases with height. This is due to the fact that the size of the triangular-shaped region, which confines the maximum energy point, is constant. Since for most applications of particle focusing it is more desirable to have the focal point in the middle of the channel, we fabricated our device with a height of 100 μm. This ensures that the focal point is nearly in the middle of the channel.

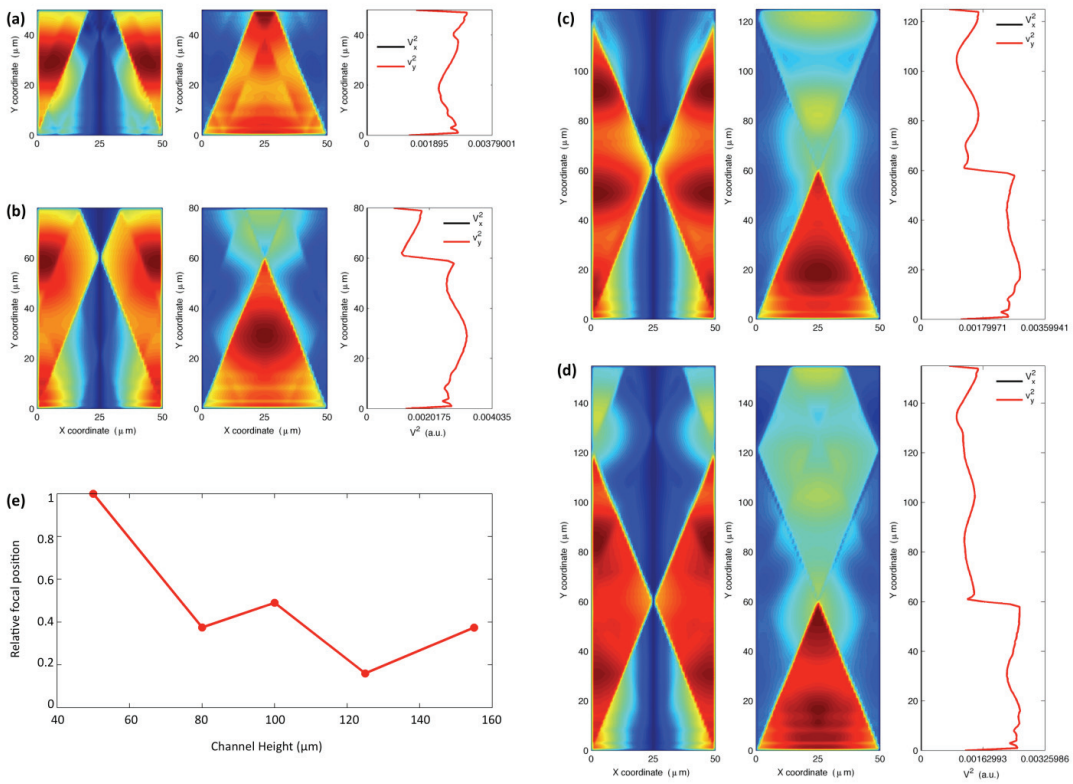

Fig. S2 Simulation results of time-averaged velocity squared field in the *x*-direction (V_x^2), *y*-direction (V_y^2), and time-averaged velocity squared in the *x*-direction (V_x^2) and *y*-direction (V_y^2) within the middle plane (x =25 μm) is plotted for various channel heights (a) 50 μm, (b) 80 μm, (c) 125 μm, and (d) 155 μm. (e) Position of the focusing point (in the *y*-direction) normalized by the channel height versus the channel height is plotted.

4. Parameters used in the simulations

Our ray-tracing based model takes full account of the attenuation of waves propagating in different media ($LiNbO_3$ substrate and water) and reflections from channel walls to assure the reliability of the simulated results. All the parameters were set to match the exact conditions in our experiments. For example, the reflection coefficient of longitudinal waves from the channel walls were obtained using the acoustic impedance of water and PDMS or $LiNbO_3$ and the incident angle using the following equation:

$$R = \frac{(z_2/z_1)-\sqrt{1-[n-1]tan^2\theta}}{(z_2/z_1)+\sqrt{1-[n-1]tan^2\theta}},$$

where z is the acoustic impedance and θ is the incident angle. The calculated values of reflection for the side, top, and bottom wall are 50%, 23%, and 99%, respectively. Figure S3 shows a schematic of the leakage waves entering the channel and reflecting from the channel walls. Table 1 shows the parameters that were used in the simulations. The leakage rate of surface waves is calculated using equation (15) of ref. S2.

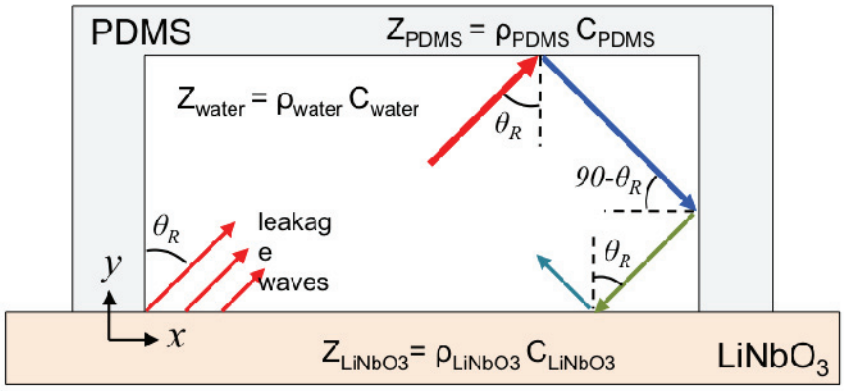

Fig. S3. Schematic of the SAW entering the microfluidic channel under the Rayleigh angle. The leakage wave attenuates as it travels within the media and reflected from the channel walls.

Table 1. Values for parameters used in the simulations

Parameter	Value
Longitudinal wave velocity in water	1490 (m/s)
Density of water	1000 (kg/m^3)
Compressibility of water	4.48e-10 $(1/Pa)$
Attenuation coefficient in water	0.23222 $(dB/(MHz.cm))$
Longitudinal wave velocity in PDMS	1020 (m/s)
Density of PDMS	965 (kg/m^3)
Attenuation coefficient in PDMS	3.3457 $(dB/(MHz.cm))$
Density of spherical particle	1053 (kg/m^3)

Compressibility of spherical particle	2.16e-10 $(1/Pa)$
Diameter of spherical particle	1.9e-6 (m)
Longitudinal wave velocity in LiNbO3	7150 (m/s)
SAW velocity of LiNbO3 on 128 Y-cut, x-direction	3900 (m/s)
Density of LiNbO3	4650 (kg/m^3)

5. Transverse primary radiation forces

The working mechanism of particle focusing using standing acoustic waves is based on the balance of acoustic radiation forces. However, the magnitudes of the radiation forces in the lateral and vertical directions are functions of different parameters. In the main text, we explained that the particles go to pressure nodal planes because of axial primary radiation forces (in the lateral direction). The balance of these forces determines the particles' lateral position.

The vertical position of the particles is dictated by the transverse radiation forces which are function of the gradient in the acoustic energy field. The equation from which the transverse force is determined is shown here:

$$F = V_0 \nabla E_{ac} \left(\frac{3(\rho_p - \rho_f)}{\rho_f + 2\rho_p} cos^2(ky) - \frac{\beta_f - \beta_p}{\beta_f} sin^2(ky)\right).$$

In this equation V_0 is the static particle volume. β and ρ are, respectively, compressibility and density of the fluid (f) and particle (p). E_{ac} is the acoustic energy density which is the sum of time-averaged kinetic and potential energy. Due to axial radiation forces, particles are placed in the pressure nodal plane. On this plane the pressure and the potential energy are zero. Therefore, acoustic energy density is only determined by time-averaged kinetic energy which is a function of velocity squared. [S3,S4]

References:

S1. Optimal Protocol for Molding PDMS with a PDMS master, Chips & Tips, Lab on a Chip.

S2."Lens Design for Acoustic Microscopy," IEEE Transactions on Ultrasonics, Ferroelectrics and Frequency Control, Vol. 35, No. 4, July 1988.

S3.M. Woodside, B. D. Bowen, and J. M. Piret, AIChE J., 1997, 43, 1727-1736.

S4.C. J. Schram, in Advances in Sonochemistry: Manipulation of particles in an acoustic field, T.J. Mason, Elsevier, 1991, pp. 293-322.